Minimizing Wireless Delay with a High-Throughput Side Channel

Ruirong Chen, *Student Member, IEEE*, Haoyang Lu, *Student Member, IEEE*, and Wei Gao, *Member, IEEE*

Abstract—Performance of modern cognitive and interactive mobile applications highly depends on the transmission delay in the wireless link that is vital to supporting real-time wireless traffic. To eliminate wireless network congestion caused by large amounts of concurrent network traffic and minimize such transmission delay, traditional schemes adopt various flow control and QoS-aware traffic scheduling techniques, but fail when the amount of network traffic further increases. In this paper, we present a novel design of high-throughput wireless side channel, which operates concurrently with the existing wireless network channel over the same spectrum but dedicates to real-time traffic. Our key idea of realizing such a side channel is to exploit the excessive SNR margin in the wireless network to encode data as patterned interference. We design such patterned interference in the form of energy erasure over specific subcarriers in an OFDM-based wireless network, and achieve a data rate of 1.25 Mbps in the side channel without affecting the existing wireless network links. Experimental results over both software-defined radios and custom wireless hardware demonstrate the effectiveness of our side channel design in reducing the latency of real-time wireless traffic, while providing a sufficient data throughput for such traffic.

Index Terms—Wireless networks, wireless side channel, real-time wireless traffic

1 Introduction

Mobile computing has been an indispensable part of every aspect of modern life, by enabling highly cognitive and interactive mobile applications over heterogeneous types of mobile devices. Representative examples of these mobile applications include mobile cloud computing [28], resource sharing among mobile systems [3], wearable and edge computing [16], [51], and multi-party mobile gaming [27], [29], [30], which fundamentally transform the way people access information and interact with each other. Performance of these applications depends on the latency of wireless links connecting mobile devices with each other and the remote cloud, support real-time wireless traffic that is vital to prompt application response.

In practice, the real-time wireless traffic of these applications may be seriously delayed when competing with other data traffic being transmitted concurrently over the same wireless channel. Traditional designs of wireless networks eliminate such network congestion via Quality of Service (QoS)-aware traffic scheduling [5], [34] or flow control [7], but fail when the amount of network traffic further increases. Another option to alleviate such network congestion is to allocate additional wireless spectrum that is exclusively used for real-time wireless traffic. For example, a dedicated spectrum is designated as the control plane in cellular networks [33]. However, such exploitation of additional spectrum is infeasible due to the spectrum scarcity nowadays.

Instead, another viable solution to removing this fundamental limitation on supporting real-time wireless traffic is to explore *a wireless communication side channel*, which operates concurrently with the existing wireless channel[1] over the same spectrum but dedicates to transmitting real-time traffic. When the main channel is congested, real-time traffic is transmitted through the side channel. Hence, communication of delay-sensitive applications between mobile devices will never be delayed by concurrent wireless traffic, and its latency only depends on the link propagation delay. The key insight of such a side channel is that the Signal-to-Noise Ratio (SNR) of a wireless channel is usually higher than the SNR required to support the data rate being used, due to inaccurate SNR estimation and conservative rate adaptation in wireless networks. This in-band *SNR margin* can be exploited to encode data as *patterned interference* over the main channel. The impact of such a side channel on packet decoding over the main channel, on the other hand, could be efficiently eliminated by limiting the amount of additional patterned interference within the scope of the main channel's SNR margin.

In order to support real-time wireless traffic, the wireless side channel has to provide sufficient data throughput that is required by modern interactive mobile applications. Existing schemes have designed the side channel over commodity wireless networks such as WiFi [8] and ZigBee [54], but are limited to achieving a data throughput of several hundreds of kbps. This side channel, hence, can only be used to transmit small network control messages (e.g., RTS/CTS frames) but is

• *The authors are with the Department of Electrical and Computer Engineering, University of Pittsburgh, 3700 O'Hara Street, Pittsburgh, PA 15261. E-mail: {ruc28, hlu9, weigao}@pitt.edu.*

Manuscript received 30 Jan. 2018; revised 21 Mar. 2019; accepted 17 Apr. 2019. Date of publication 30 Apr. 2019; date of current version 3 June 2020. (Corresponding author: Ruirong Chen.)
Digital Object Identifier no. 10.1109/TMC.2019.2914048

1. The existing channel being used in current wireless networks is denoted as the "main channel" throughout the rest of this paper.

far from sufficient for mobile application traffic. Further improving the side channel throughput, in theory, needs to encode more bits into the patterned interference. Such throughput improvement, however, is difficult because the amount of interference that can be exploited for data encoding is limited by the channel SNR margin.

In this paper, we present a practical high-throughput design of the wireless side channel that efficiently supports real-time wireless traffic over heavily congested wireless channels, by exploiting the unique properties of modern digital modulation methods, particularly OFDM which will be the technical foundation of next-generation high-speed wireless networks (e.g., LTE-A and 5G) [52]. Our basic idea of the side channel design is to encode data as patterned interference by erasing the energy of specific subcarriers in the main channel's OFDM symbols. Since such energy erasure does not increase the RF transmit power, it can be used to encode data into every OFDM symbol in the main channel, hence dramatically increasing the side channel throughput. On the other hand, since OFDM modulates data into separate subcarriers in both time and frequency domains, the amount of patterned interference could be efficiently controlled by interfering only a small portion of OFDM subcarriers, without affecting main channel decoding and its resistance to channel contention.

The major challenges of such high-throughput side channel design, however, are two-fold. First, it is hard to ensure precise detection of patterned interference in the form of energy erasure over OFDM subcarriers, which can be easily corrupted by the channel noise. A straightforward solution is to detect energy erasure as the subcarrier with the minimum level of energy. However, when the channel noise is sufficiently high, it may increase the energy level of the erased subcarrier and hence results in detection errors. Second, our proposed design also raises unique challenge to channel operation and control. It is difficult to distinguish data transmitted in the side channel from background noise, without knowing the existence of such a side channel in advance. Lightweight techniques for connection establishment over the side channel are hence needed without continuous detection of patterned interference.

To overcome the aforementioned challenges, we first propose a probabilistic approach to detecting patterned interference, which takes the channel noise model into account and achieves a high detection rate over the side channel. This approach is also resistant to the multipath channel fading and ambient noise. We then indicate the existence and the destination of a wireless side channel by exploiting the idle time periods between data frames in the main channel and inserting a specialized preamble between these frames. This approach, therefore, does not require active cooperation of the main channel and will not be affected by the traffic status in the main channel.

We have implemented the proposed system design over both Software-Defined Radios (SDR) and WARP hardware platform, and evaluated the effectiveness of our design over different wireless frequency bands and realistic wireless applications. The experimental results show that our system can provide a side channel throughput of up to 2.5 Mbps, which is 10 times higher than existing work with minimal impairment to the main channel performance. It also reduces the delay in commodity 802.11 networks by up to 90 percent, and significantly eliminates the chance of delay jitters in such networks. Such delay reduction and throughput enhancement enable many delay-sensitive mobile applications, e.g., Skype, to operate in the side channel without any performance degradation even if the main channel is highly congested. The traffic from these applications, meanwhile, can be supported by the side channel without impairing the main channel performance.

The rest of this paper is organized as follows. Section 2 reviews the existing work. Section 3 gives a brief overview on our design. Sections 4 and 5 present technical details of the designs of the side channel and connection establishment. Section 6 evaluates the performance of our system over the SDR platform via network emulation. Sections 7 and 8 further present details of our implementation and performance evaluation over the WARP hardware platform. Finally, Section 9 discusses and Section 10 concludes the paper.

2 Related Work

To efficiently eliminate the network congestion, various QoS control schemes have been proposed to prioritize delay-sensitive network traffic [42], and the TCP flow control also helps reduce the channel congestion [26]. However, these designs cannot scale to the increase of network traffic. Other schemes, such as mm-wave networking [21], [45], multiuser MIMO [38], channel bonding [25], beamforming [44] and continuous link rates [35], strive to alleviate the network congestion by further enhancing the wireless throughput, but require either new spectrum or additional hardware. Recent schemes in wireless network scheduling provide MAC-layer solutions to network congestion based on carrier-sense multiple access [4], [9] that allows multiple wireless devices to access the network in turn, but fails when the amount of network traffic and the corresponding contention for channel access scale up. Researchers also suggested to design wireless networks as rateless to maximize the channel throughput, i.e., the link rate continuously varies based on the channel condition without any explicit channel feedback [14]. However, these rateless networks incur extra communication and computation overhead that are generally unaffordable by the resource-constrained wireless devices.

Instead, recent studies aim to reduce the transmission latency by exploiting extra communication opportunities beyond the existing wireless channel. Existing designs of the in-band side channel are mainly applied for delivering coordination and control information, so as to improve the network performance without introducing extra costs compared to the out-of-band approaches. The side channel conveying the control messages is operated concurrently with data transmissions in the main channel, without jeopardizing the latter's performance. Wu et al. [54] observes the underutilization of interference-tolerance provided by most physical layer implementations, and encodes a small amount of control messages by intentionally interfering several chips in each ZigBee symbol. Flashback [8] builds a control plane with a 400 kbps data rate in OFDM-based WiFi packets, by interpolating high-energy spikes into OFDM subcarriers. These spikes transmit at a power level that is 64 times greater than the power used for regular data symbols, hence allowing easier detection. However, all these designs are limited to conveying the small-size network control messages over the low-throughput side channels. In contrast, the major focus of this paper is to develop a side channel with a throughput that is sufficiently high to support real-time wireless traffic of

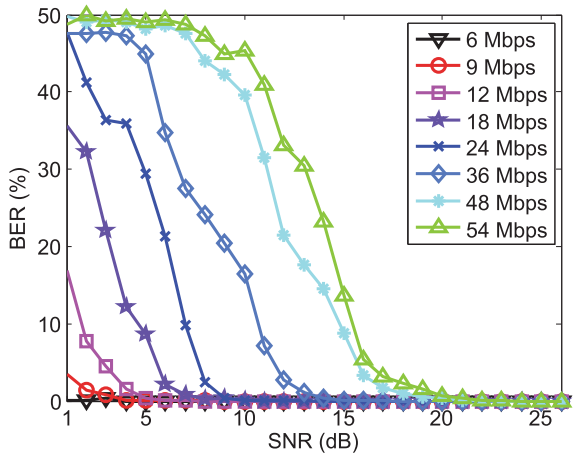

Fig. 1. Channel BER under different SNR conditions.

mobile applications when the main channel is congested. We build our side channel upon commodity WiFi standard and achieve a high throughput by interfering one or more subcarriers in every OFDM symbol.

Orthogonal Frequency-Division Multiple Access (OFDMA) [10], a multi-user version of the OFDM design, can be potentially used as an alternative of the side channel, by dedicating a certain amount of subcarriers exclusively for the delay-sensitive traffic. However, the channel throughput for other traffic will inevitably suffer from degradation. For example, if two subcarriers are dedicated to delay-sensitive traffic, the throughput degradation for other traffic will be degraded 4 percent (2/48). In addition, since our design is implemented at the PHY layer and requires no modification of MAC, it can also work in parallel with other advanced MAC-layer network standards such as 802.11e [23], which prioritizes the delay-sensitive traffic at the MAC. Applications which require immediate responses such as workload offloading in the mobile cloud [11], [12], [50], furthermore, can also benefit from our work.

Another alternative of the side channel, as suggested by recent studies, is Cross-Technology Communication, which addresses wireless network congestion by allowing different wireless technologies to explicit coordinate their transmissions with each other. FreeBee [22] enables cross-technology communication by adding a modulated beacon that can be demodulated from different devices. WEBee [31] further extended this technique by using a software to emulate Zigbee packets from WiFi devices, and B2W2 [6] enables concurrent communication among multiple WiFi and Bluetooth devices by embedding a Bluetooth message into its overlapped WiFi subcarriers. However, the data rate achieved by these techniques is also very limited. Instead, our side channel design could provide a much higher throughput in the side channel with ultra-low latency, and hence could satisfy the requirements of many delay-sensitive applications on wireless bandwidth.

Our design for connection establishment and control in the side channel is partly inspired by another type of the side channel design, which is achieved through appending preambles to the wireless channel. E-Mili [56] constructs the M-preamble to facilitate the sampling-rate invariant packet detection, so that the WiFi receivers could recover from the downclocked idle listening mode once a valid preamble is received. The M-preamble is comprised of duplicated versions of complex Gold sequences (CGS), whose length implicitly conveys the address information. Gap Sense [57] allows a interaction between mobile devices with heterogeneous types of wireless networks, by prepending legacy packets with a preamble consisting of multiple energy pulses with quiet periods in between. This quiet period conveys control messages, and can be detected by neighboring nodes with incompatible physical layers. Being different from existing schemes which develop new preambles and hence require specialized hardware or software to operate these preambles, our approach uses a simple duplication of regular WiFi preambles. The presence of the side channel preamble indicates the availability of the side channel, and if available, the interval between the side channel preamble and the regular WiFi preamble conveys the address of the side channel recipient. Hence, our schemes could be easily deployed over commodity WiFi transceivers.

3 Overview

In this section, we first elaborate our motivation of developing a side channel for supporting real-time wireless traffic, by demonstrating the existence of SNR margin in practical wireless channels. Next, we briefly introduce the background of the OFDM-based WiFi physical layer standard. Finally, we present the high-level picture of our proposed side channel design.

3.1 Motivation

As described above, our major motivation of designing the wireless side channel is the existence of SNR margin in the wireless channel, i.e., the difference between the actual channel SNR and the minimum channel SNR that is required to support the channel data rate being used. Although most rate adaptation algorithms being used in practical wireless networks do not directly decide the data rate based on the channel SNR, such data rate is closely correlated to SNR that decides whether packets can be successfully received and decoded. For example, Auto Rate Fallback (ARF) [37] adjusts the data rate according to the statistics of packet loss in the past, and Receiver Based AutoRate (RBAR) [17] chooses the data rate based on the average SNR of successfully transmitted packets.

To further evaluate the amount of such SNR margin in practical WiFi networks, we conduct a preliminary experiment over USRP N210 SDR boards with GNURadio toolkit.[2] More specifically, we emulate different levels of channel SNR at the sender side by adjusting the transmit gain of the sending USRP board. At the receiver side, we estimate the channel status at real-time and compute the BER by comparing the received data frames with expected ones. The experiment results in Fig. 1 show the relationship between channel SNR and BER when different data rates are being used.[3] For example, it shows that 5.8 dB is the minimum required SNR for the 9 Mbps data rate and 7.9 dB for the 12 Mbps data rate, and the SNR margin is hence 2.1 dB. In practice, such margin is decided based on the gap between different data rate curves in Fig. 1. This SNR margin will further increase when the wireless channel condition improves and a higher data rate is adopted due to the bigger gap between data curves. When the data rate increases to 48 Mbps, the SNR margin will be 5 dB.

2. http://gnuradio.org/redmine/projects/gnuradio

3. Different data rates are adopted by using different modulation methods and code rates. For example, 6 Mbps is realized by BPSK with the code rate 1/2.

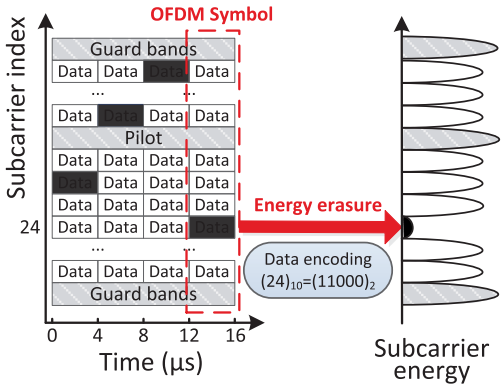

Fig. 2. Encoding data as patterned interference into an OFDM symbol.

The existence of such SNR margin, therefore, validates our proposed side channel design. Particularly, note that traditional designs of wireless side channels only exploit a small portion of the SNR margin to deliver the small-size control messages. In contrast, we envision that the SNR margin can be further exploited to increase the throughput of the side channel without impairing the performance of the main channel. The key challenge, however, is how to appropriately limit the amount of patterned interference being applied.

3.2 OFDM Primes

Our proposed design of the wireless side channel builds on Orthogonal Frequency Division Multiplexing (OFDM), which is a multicarrier modulation technique and is widely used in existing WiFi and cellular networks because of its high efficiency of spectrum utilization and resistance to multipath channel fading and inter-carrier interference. Data in OFDM is transmitted concurrently in closely spaced subcarriers, each of which corresponds to a frequency band that is orthogonal to others. Specifically, each 20 MHz WiFi channel comprises of 64 OFDM subcarriers that are spaced 312.5 kHz apart. In an OFDM symbol in the IEEE 802.11a standard, 12 subcarriers (including DC) are null as the guard band, 4 subcarriers are occupied by pre-known pilots for frequency offset compensation, and 48 subcarriers are used for data transmission. The duration of each OFDM symbol is 4 μs.

As a result, one OFDM packet could be viewed as a two-dimensional time-frequency grid, as shown in Fig. 2. All data subcarriers within one packet use the same modulation symbol mapper (e.g., BPSK, QPSK, 16-QAM or 64-QAM) and the same code rate (e.g., 1/2, 2/3 or 3/4), according to the data rate being adopted. Different settings of the modulation symbol mapper approach and code rate yield different data rates and the anti-interference capability. For example, BPSK with 1/2 code rate yields the lowest 6 Mbps data rate but is the most resistant to noise, and is hence adopted in poor SNR scenarios. On the contrary, 64-QAM with 3/4 code rate provides the maximum 54 Mbps throughput by using a denser constellation diagram, and is applied in good SNR scenarios.

In each OFDM symbol, inverse FFT is applied to transform the signal from the frequency domain into the time domain. The symbol mapped into each subcarrier thereby can be viewed as a combination of the magnitude and phase information, or frequency response of that particular subcarrier. Therefore, if we manually replace the original data in one subcarrier with "0", it is equivalent to erasing the power in that subcarrier. This characteristic will be the foundation of our side channel design which applies patterned interference onto OFDM subcarriers via energy erasure.

3.3 Big Picture

As shown in Fig. 2, our primary design of the side channel is to erase the energy of one specific subcarrier in each OFDM symbol. At the sender's side, the patterned interference is only applied to one OFDM subcarrier in each symbol, and hence controlled within the scope of channel SNR margin. At the receiver's side, an erased subcarrier can be detected as the subcarrier with minimum level of energy. Since we do not require any additional hardware or increase the RF transmit power, little energy consumption is incurred by the side channel. As a result, when we erase the energy of one of the 48 OFDM subcarriers,[4] $\lfloor \log_2 48 \rfloor = 5$ data bits can be encoded into each symbol and the maximum data rate of the side channel is $5b/4\,\mu\text{s} = 1.25$ Mbps. For example in Fig. 2, erasing subcarrier 24 transmits data $(11000)_2$ over the side channel. In practice, this data rate depends on the accuracy of detecting patterned interference, and we propose a probabilistic approach to ensure the precise detection of such interference in Section 4.

In our side channel design, the main channel information modulated in the subcarriers being erased is unrecoverable, which could potentially impact the performance of the main channel. However, such impact could be efficiently controlled and mitigated if prior knowledge of the corrupted (erased) subcarriers is available. More specifically, the wireless receiver first detects the OFDM subcarriers being corrupted by the side channel before feeding the OFDM symbols to the Viterbi decoder in the main channel. Then, the Viterbi decoder in the main channel could utilize such information to reduce the weight of those bits contained in the corrupted subcarriers when doing its best-path search, known as the erasure operation, so as to avoid decoding error and data packet corruption.

4 Side Channel Design

In this section, we first describe the overall system design of the wireless side channel, which requires the minimum hardware modification over commodity WiFi networks. Then, we present the probabilistic approach to detecting patterned interference, which ensures the detection rate of patterned interference in a wireless channel with additive white Gaussian noise (AWGN).

4.1 Overall System Design

The system architecture of the side channel over WiFi networks is shown in Fig. 3. Specifically, the real-time traffic is denoted as D' and conveyed in the side channel, and other network traffic is denoted as D and transmitted in the main channel. Energy erasure of OFDM subcarriers is implemented through a simple masking and multiplication approach. More specifically, in the transmitter side, a Pulse Position Modulator (PPM) [46] is applied onto D'. Correspondingly, a sequence of binary numbers, denoted as the mask M, is generated with '1' and '0' referring to either reserve or erase the energy in a specific subcarrier. For example, in Fig. 2, erasing the energy of the 24th OFDM subcarrier, which corresponds to encode data $(11000)_2$ in the side channel, maps to the following mask:

4. Four pilot subcarriers are not used.

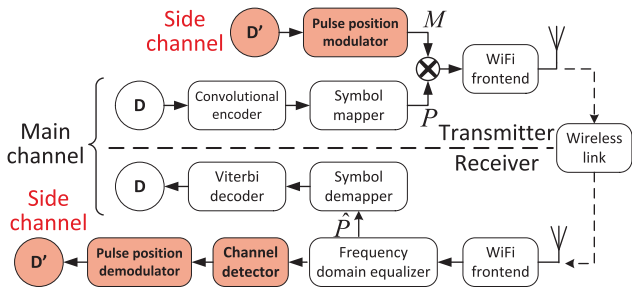

Fig. 3. Side channel design over WiFi networks.

$$\underbrace{1}_{c_{31}}\,1\ldots1\,\underbrace{0}_{c_{24}}\,1\ldots1\,\underbrace{1}_{c_0}. \tag{1}$$

This mask contains a single '0' in the position of c_{24}, and is then applied on the main channel subcarriers, which is equivalent to erasing subcarrier c_{24} while maintaining all other ones unchanged.

Based on such scheme, the wireless network system consisting of both a main channel and a side channel works as follows. First, the modulation process in the main channel remains unchanged. As shown in Fig. 3, the convolutional encoder, which uses one type of the Forward Error Correction (FEC) coding scheme, introduces redundancy into the modulation process for error correction. The symbol mapper transforms the binary sequence to a sequence of constellation points P, according to the modulation methods being used. After the masking procedure, the carrier mapper would assemble an OFDM packet by filling the data sequence into the time-frequency grids. The FFT module then transforms the data from frequency domain to time domain for transmission. Second, at the receiver side, the signal distortion introduced by multipath fading is compensated by the frequency domain equalizer, by measuring the misshaping of the pre-known long training sequences. The packet $\hat{P}$ after equalization is then fed to the symbol demapper and Viterbi decoder for demodulation, and to the side channel detector for detection of the erased subcarriers. The side channel information D' is then recovered through pulse position demodulator.

Since our design retains the OFDM-based PHY and the other layers in the main channel unchanged, it only involves a minimum amount of modification to the existing WiFi hardware. We will further elaborate such hardware modification in more detail in Section 7.

4.2 Improvement of Data Throughput

Based on this basic design of the side channel, the major approach to further improve the data throughput of the side channel is to erase multiple subcarriers in an OFDM symbol. Let K be the number of subcarriers being erased in each OFDM symbol, the number of data bits in the side channel that can be transmitted per symbol is hence $\lfloor \log_2(C_{48}^K) \rfloor$, which will quickly increase along with the value of K. For example, a throughput of 2.5 Mbps can be achieved by erasing two subcarriers per OFDM symbol. Essentially, this scheme improves the data throughput of the side channel by increasing the amount of patterned interference applied to the main channel. Since such interference is applied as energy erasure, its amount can be arbitrarily increased, in theory, without breaching the radiation power limit.

However, increasing the amount of patterned interference improves the side channel throughput at the cost of increasing the decoding errors and BER in the main channel, as more information being transmitted is removed from the main channel. Therefore, to efficiently control the amount of patterned interference within the scope of channel SNR margin, we limit $K \leq 2$ (4.1 percent subcarriers) in our design. In practice, the value of K is declared in the SIGNAL symbol in a regular WiFi frame. According to the 802.11 standard [2], the SIGNAL symbol is the first symbol after preambles, followed by DATA symbols, determining the data rate and the length of the frame. To ensure reliable delivery, the SIGNAL symbol is always transferred in the lowest data rate, e.g., 6 Mbps using BPSK. Similarly, we apply the lowest data rate ($K = 1$) in the SIGNAL symbol, to encode the information about the side channel data rate being used over the subsequent DATA symbols.

4.3 Probabilistic Detection of Energy Erasure

Precise detection of patterned interference in the form of energy erasure is the vital factor that determines the performance of both the main channel and the side channel. Detection errors not only reduce the throughput of the side channel, but also increase the main channel BER by misinforming the Viterbi decoder to erase the correct main channel bits while keeping the corrupted bits. The impact of such detection errors is even more severe when multiple subcarriers are being erased.

The major challenge hindering precise detection of patterned interference is channel noise. When sufficient noise exists in the erased OFDM subcarrier, this subcarrier may not be the one with the minimum level of energy and result in detection error, when the straightforward detection approach presented in Section 4.1 is being used. According to [43], the received signal Y in the frequency domain (after FFT) can be written in time-frequency matrix notation as

$$\boldsymbol{Y} = diag(\boldsymbol{X})\boldsymbol{H} + \boldsymbol{N}, \tag{2}$$

where $\boldsymbol{N}$ is AWGN noise and $\boldsymbol{H}$ is the Fourier Transform of the system function of the multipath channel $h(\tau)$. Since OFDM can efficiently reduce the impact of multipath fading by adopting the low-rate symbols and the pilot-based frequency-domain equalization [32], [55], we consider the AWGN as the major source of the distortion.

Based on such modeling of channel noise, our basic idea of improving the detection accuracy is to probabilistically evaluate the chance for each OFDM subcarrier to contain the patterned interference, and determine such probabilities based on subcarriers' energy levels and up-to-date characteristics of channel noise. We denote $\mathcal{S}$ as the set of points on the constellation diagram corresponding to the digital modulation method used in the main channel, and X and Y as the constellation symbols of the transmitted and received signals in a subcarrier, respectively. From the viewpoint of constellation diagram, the procedure of the subcarrier erasure is equivalent to designating an extra constellation point, i.e., the origin $O = (0, 0)$, to the side channel signals. Therefore, $X \in \mathcal{S} \bigcup O$. Then, the posterior probability for this subcarrier to contain the patterned interference can be calculated by the receiver as

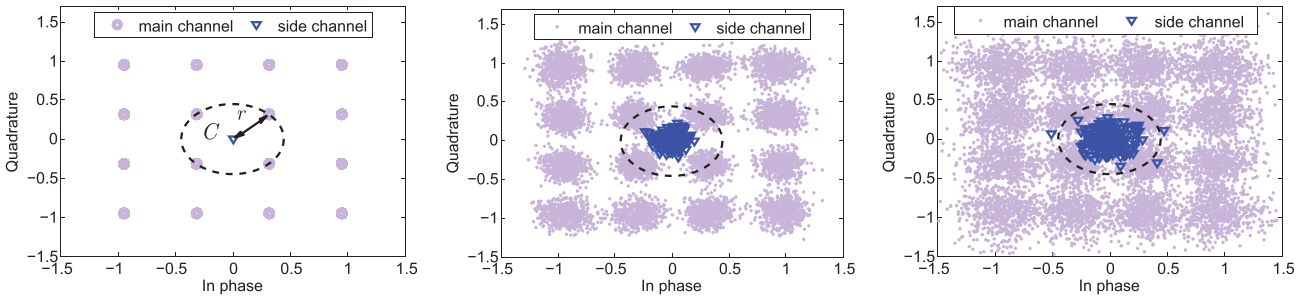

(a) Noise-free scenario (b) Received signal (18 dB) (c) Received signal (14 dB)

Fig. 4. Constellation diagram of 16-QAM (3/4) under different channel SNR conditions.

$$\mathbb{P}\{X = O|Y\} = \frac{\mathbb{P}\{Y|X = O\} \cdot \mathbb{P}\{X = O\}}{\sum_{s \in \mathcal{S} \bigcup O} \mathbb{P}\{Y|X = s\} \cdot \mathbb{P}\{X = s\}}. \quad (3)$$

When there is no channel noise, Y always equals to X and the subcarrier with the minimum energy always contains the patterned interference. Otherwise, the smaller Y is, the higher probability is computed in Eq. (3). The prior probability of $\mathbb{P}\{X = O\} = \frac{K}{N}$ where N is the number of OFDM subcarriers that are used to transmit data in the main channel. $\mathbb{P}(X = s) = 1/|\mathcal{S}| \cdot (1 - K/N)$ for all $s \in \mathcal{S}$. With AWGN, the conditional probability $\mathbb{P}\{Y|X = s\}$ can be computed from a two-dimensional Gaussian distribution $\mathbb{N}(\boldsymbol{\mu}, \boldsymbol{\Sigma})$ with $\boldsymbol{\mu} = O$, based on the distance between X and Y in the complex plane. The noise level is reflected by the Gaussian co-variance matrix $\boldsymbol{\Sigma}$, which correlates to channel SNR and is continuously estimated at real-time [40].

Since Eq. (3) computes $\mathbb{P}\{Y|X = s\}$ for every $s \in \mathcal{S} \bigcup O$, such probabilistic detection of patterned interference with a higher order modulation incurs a additional computational overhead. For example, the above probability needs to be computed 65 times if 64-QAM modulation is applied. To reduce such overhead, we investigate the spacial distribution of the erased subcarriers in the constellation diagram. As shown in Figs. 4b and 4c, with a moderate channel condition where the main channel information could be correctly decoded, almost all the received side channel signals in the constellation diagram are within the circle C that centers on the origin, whose radius r is the distance between origin and its closest constellation point in the main channel. In other words, the side channel signals are very likely to be falsely classified as the main channel signals with the lowest power in poor SNR scenarios.

In this case, we only need to concern about the received signals with a magnitude less than r, and classify the others as the main channel data. We hence replace the set $\mathcal{S}$ with $\mathcal{S}'$ in the denominator of Eq. (3), where $\mathcal{S}'$ only consists of the weakest main channel signals in the constellation diagram. $\mathcal{S}'$ contains at most 4 elements (2 elements for BPSK), which significantly reduces the computational workload of our detection approach.

5 Connection Establishment and Transmission Control

In our design, since data is transmitted over the side channel as patterned interference, it is difficult to distinguish the side channel from background noise, without knowing the existence of such a side channel in advance. Lightweight techniques for connection establishment over the side channel are hence needed without continuous detection of the patterned interference. In this section, we indicate the existence and destination of a side channel by appending a specialized preamble to the regular data frames in the main channel, so as to facilitate connection establishment and transmission control in the side channel.

5.1 Connection Establishment

We enable lightweight connection establishment over the side channel by exploiting the idle time periods between data frames in the main channel. For example, the 802.11 standard requires a DCF Interframe Space (DIFS) of 34 μs between every two WiFi frames [36], [56]. More specifically, each OFDM-based 802.11 data frame starts with Short Training Sequences (STSs), which consists of 10 duplicate short symbols spanning 16 samples, i.e., 0.8 μs in a 20 MHz bandwidth system each. The frame detection, together with the Automatic Gain Control (AGC) and the timing synchronization, is achieved by computing the auto-correlation of STS. Hence, as shown in Fig. 5a, we indicate the existence of the side channel by placing a special preamble, as a set of STSs, to the idle period between two main channel frames.

Since a STS is the beginning indicator of a WiFi frame, it can be efficiently detected by the embedded WiFi AGC via auto-correlation without any additional hardware. Such auto-correlation exploits the cyclic characteristic of STSs and takes the power level of the received signal into consideration [41]. In WiFi systems, a new data frame is considered to be detected once the auto-correlation coefficients $c[n]$ of N consecutive samples exceeds the threshold C_{th}. The special preamble indicating the side channel existence, hence, can be detected in the same way. From Fig. 5b which demonstrates such auto-correlation process with 10 dB of channel SNR, we can see that this special preamble can be efficiently distinguished from the data frame in the main channel, even in low-SNR scenarios.

5.2 Side Channel Addressing

The destination of a side channel may be different from that of the main channel. Hence, we encode the information about the traffic destination of the side channel as the relative time location (L) of the special preamble in the idle period between data frames. The address information is represented as

$$Address = (L - L_{guard} - L_{Preamble})/D, \quad (4)$$

where L_{guard} is the guard interval between the special preamble and the regular WiFi frame, $L_{Preamble}$ is the duration of the special preamble, and D is the resolution of preamble

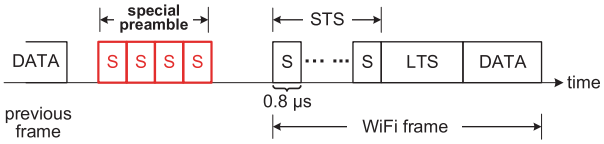

(a) Preamble design

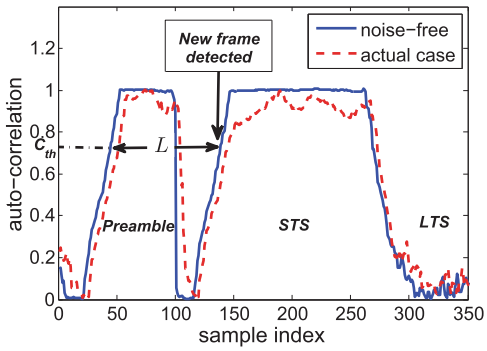

(b) Preamble detection via auto-correlation

Fig. 5. Design and detection of the side channel preamble.

detection. When $L_{guard} = L_{Preamble} = 0$ and D equals to 10 WiFi samples (0.5 μs), the WiFi receiver can distinguish $34\,\mu s/0.5\ \mu s = 68$ different time locations in the idle period, allowing $\lfloor \log_2 68 \rfloor = 6$ data bits being encoded and a maximum number of $2^6 = 64$ devices to be interconnected at the same time. These data bits could also be used to transmit data acknowledgments that are necessary for reliable data transfer.

The actual amount of data bits being encoded also depends on the values of L_{guard} and $L_{Preamble}$. A small L_{guard} or a large $L_{Preamble}$ would mistakenly indicate an immediate start of regular frame, leading to frame detection error in the main channel. On the contrary, a large L_{guard} reduces the number of data bits being encoded, and a small $L_{Preamble}$ makes the preamble detection prone to channel noise. By experimentally investigating with the off-the-shelf WiFi receivers, we found the preamble consisting of 2 STSs with a guard time of 10 samples is the most suitable design choice for the wireless side channel.

6 Performance Evaluation over Software-Defined Radios

In this section, we evaluate the performance of our proposed side channel design over USRP/GNU Radio platforms. The metrics being used in our evaluations include the data transmission delay, the channel throughput, and the detection rate of patterned interference.

6.1 System Implementation and Experiment Setup

We implemented our design over USRP SDR boards with the GNURadio toolkit, which realize an 802.11a WiFi transceiver over the 5.85 GHz frequency band. USRP N210 motherboards and UBX 40 RF daughterboards are used, which operates in the range between 10 MHz and 6 GHz. Both AP and client are implemented with USRP and a host PC. In the main channel, the frame generation follows the IEEE 802.11a standard [2]: the first OFDM symbol of each frame stores 3-byte Physical Layer Convergence Protocol (PLCP) header indicating the length and data rate of the frame, followed by the MAC Protocol data unit (MPDU) where a random sequence of strings is located onto its frame body. For each OFDM symbol, 32 subcarriers with index -24 to 11 are exploited for the side channel, excluding the DC (index 0) and pilot (index -21 and ± 7) subcarriers.

We use this implementation to conduct experiments in a $5\,\mathrm{m} \times 5\,\mathrm{m}$ office which contains rich multipath fading effect. The sender and the receiver are placed out of line of sight and 4 meters away from each other. We tune the channel SNR by adjusting the USRP parameter of Tx Gain, which represents the RF transmit gain within a range from 2 to 30 dB. The maximum Tx power then corresponds to 13 dBm. In each experiment, 250 WiFi packets of 1 kB are synthesized and sent with an interval of 2 seconds, ensuring the timely executions of BER computation and other statistical convergence on the PC host connected to USRP boards. In addition, the noise invariance is estimated every 5 frames.

Our design is evaluated under the AP-Client mode, which is the most commonly used wireless network scenario in practice. When multiple wireless clients connected to a same AP, each of these main channel links are independently operated with existing MAC solutions. The side channels in these links, however, are also independent from each other and free of spectrum contention. The upper layer processing above MAC, such as IP and DHCP protocols, is done on host PC. Hence, our evaluation results are generic and can be applied to any larger WiFi networks with an arbitrary number of clients being connected to the same AP.

Furthermore, besides the synthesized packets being sent at a constant rate, we also evaluate our system with realistic real-time WiFi traffic, more specifically, peer-to-peer Voice over IP (VoIP) traffic. To ensure smooth conversations between endpoints, the VoIP traffic has a strict requirements on the network transmission delay: any delay exceeding 400 ms will seriously impair the quality of conversation [24]. In our evaluation, we choose to use the VoIP traffic generated by Skype, which represents the delay-sensitive applications with real-time VoIP traffic. The VoIP traffic from Skype transfers an uplink UDP packet every 20 ms, with highest data rate at 64 Kbps as specified in ITU-T standard [1]. Due to the difficulty of directly interacting between the GNURadio platform and the Skype application, we use the network sniffer Wireshark to capture the uplink Skype packets from a laptop, during which we upload large files to Google Drive to simulate congested wireless network scenarios.

6.2 Data Transmission Delay

We first evaluate the data transmission delay over the wireless side channel. In particular, we measure the round-trip delay for the sender to "ping" the receiver. To emulate the network congestion in the main channel, we generate UDP packets from multiple devices that access the main channel between the sender and receiver with commodity WiFi CSMA protocol for multiple channel access. More specifically, we use 4 UDP sockets at each device and continuously transmit packets of 1 kB every 100 ms in each socket. At the PC host operating the USRP devices, each device is operated in a separate application thread and the time for each transmission is individually recorded. Meanwhile, the same type of packets are sent through the side channel with the same interval between consecutive packets.

The round-trip data transmission delay through the main channel and the side channel from a single device is shown in Fig. 6a. When the number of devices increases in the network, the main channel is getting congested due to multiple devices' contention for channel access. More specifically, when conflicts between devices occur, a backoff timer for the backoffed device is set by the CSMA BEB (Binary Eponential

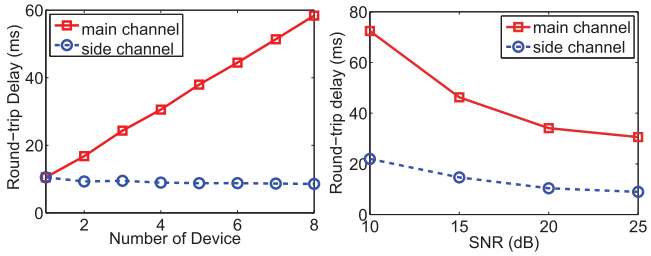

(a) (b)

Fig. 6. Data transmission delay with different congestion and SNR conditions.

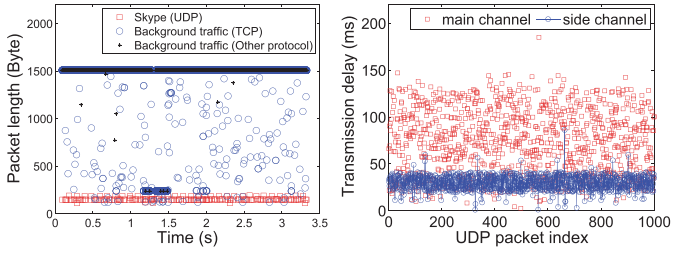

(a) Packet trace (b) Transmission delay

Fig. 7. Packet trace and transmission delay with VoIP traffic from Skype.

Backoff) algorithm that has a redoubled backoff window (CW) with the time slot $T = 20\ us$. The backoff window is set between minimal $CW_{min}T = 2T$ and maximum $CW_{max}T = 1023T$, which gives maximal backoff time at 20.46 ms. As multiple devices are contesting for channel access, the delay for all devices to compete transmission is increased significantly due to the increasing backoff time at each device and the channel queuing delay [19], [47]. Thus, the channel congestion will always occur and will further increased with more devices competing for channel access [18]. Furthermore, since each device is transmitting with the same pattern, these devices are equally contributing to the network congestion, and the amount of network congestion is always proportional to the number of transmitting devices in the network.

However, the transmission delay over the side channel remains constantly at a low level in all cases, because data delivery will never be delayed in the side channel and only experience the link propagation delay. It's noted that there is a slightly descending trend of the side channel delay with a larger number of devices in the main channel. The major reason of this descending trend is the multi-threaded decoding operations at the PC host, which affects the packet processing delay. The OS at the PC host would provide more than enough resources when multiple threads are used.

Besides, we evaluate the data transmission delay under different channel SNR scenarios, by tuning the RF Tx gain to simulate different SNR conditions. The main channel's data rate is automatically adapted to the instantaneous channel SNR, and ranges between 18 to 54 Mbps. As shown in Fig. 6b, data transmission delay in the main channel increases when the channel SNR drops, because one packet occupies the channel for long time and hence creates more channel congestion. As shown in Fig. 6a, the more congested wireless channel introduces higher delay in the main channel. In practice, the main reason for the main channel's delay to increase is the channel congestion, instead of packet loss. Hence, only when the channel SNR increases, the main channel will adapt to a higher data rate, which reduces the channel congestion and delay. Comparatively, data traffic in the side channel is only slightly affected and experiences a delay increase less than 10 ms. Such resistance to SNR degradation and fluctuation is another major advantage of our side channel design, and is important to support real-time data traffic.

The realistic VoIP traffic has also been exploited to evaluate the effectiveness of our design in supporting real-time applications in practice. The characteristics of the UDP VoIP traffic and concurrent TCP traffic, which are recorded as described in Section 6.1, are shown in Fig. 7a. After packet extraction and reconstruction, we set one USRP board as the sender to deliver the recorded packets concurrently to another two USRP boards, which are set to be the recipients of the VoIP packets and other traffic packets, respectively.

The VoIP packets are carried by the side channel and the main channel in two separate experiments for fair comparison, and the transmission delays under these two cases are shown in Fig. 7b. The results in Fig. 7b show that the side channel can effectively reduce the transmission delay by 60 percent (reducing the average transmission delay from 75.1 to 29.7 ms). This 29.7 ms delay in the side channel is much lower than the maximally allowed delay for VoIP traffic [1], and guarantees the side channel performance for delay-sensitive applications. In addition, since the side channel is dedicated to the real-time traffic, packets being transmitted in the side channel will not experience any channel contention from other ongoing traffic, and hence experience a much small delay jitter.

6.3 Detection Rate of Patterned Interference

We first evaluate the detection rate of patterned interference, when the subcarrier containing patterned interference is detected as the one with the minimum level of energy. The detection rates of such patterned interference, when one and two subcarriers are erased in an OFDM symbol, are shown in Figs. 8a and 8b, respectively. When the channel SNR is higher than 10 dB, the detection rate is nearly 100 percent with BPSK and QPSK. When higher-order modulation schemes such as 16-QAM and 64-QAM are being used, the detection rate would improve as the SNR increases, and 90 percent detection rate could be achieved under when the SNR is higher than 20 dB.

Note that in practical wireless networks, higher-order modulation schemes can only be used if the channel SNR is sufficiently high. For example, 36 Mbps can only be applied when SNR is higher than 14 dB, according to the results in Fig. 1. These experiment results in Fig. 8, hence, demonstrate high accuracy of detection in practical scenarios.

Fig. 8 shows that the detection rate of patterned interference is tightly correlated with the SNR condition, which also determines the modulation scheme being used. Such correlation can be better illustrated by Fig. 9 which plots the constellation diagrams of the received symbols in different SNR conditions. When the SNR is good as shown in Fig. 9b, all the side channel symbols are near the origin on the constellation diagram and can be accurately separated from the adjacent four constellation points used by the main channel. However, when the SNR drops, we notice from Fig. 9a that the symbols of the main channel and the side channel are mixed together and become harder to be separated. In addition, the detection rate is also affected by the modulation scheme being used. When a higher-level modulation such as 64-QAM is applied, the distance between constellation points becomes smaller,

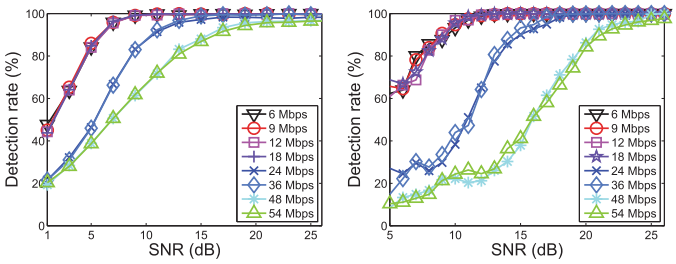

(a) Erasing one subcarrier (b) Erasing two subcarriers

Fig. 8. Detection rate of patterned interference.

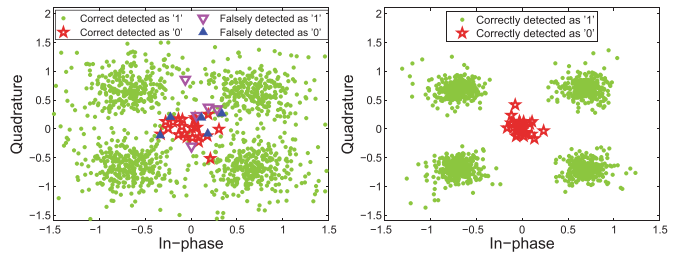

(a) 10 dB (b) 20 dB

Fig. 9. Constellation diagrams under different SNR (QPSK 3/4).

making it more difficult to differentiate between the side channel and the main channel signals.

Based on these results, we further evaluate the performance of our proposed approach in Section 4.3 to probabilistic detection of patterned interference. The evaluation results are summarized in Table 1, where (1) and (2) denote the cases in which one and two subcarriers are erased in each OFDM symbol, respectively. Generally speaking, the probabilistic approach of patterned interference detection is able to improve the detection rate by 20 percent comparing with the basic detection approach that searches for the lowest subcarrier energy, especially in low SNR scenarios.

6.4 Data Throughput of the Side Channel

Built on precise detection of patterned interference, we evaluate the data throughput of the side channel in practical network scenarios with different channel SNR conditions. The data rate currently used in the main channel is decided by the corresponding modulation scheme and code rate being used, which are closely correlated to the main channel SNR. Intuitively, the higher the channel SNR is, the more accurate the patterned interference could be detected, and hence the higher data throughput could be realized in the side channel. Table 2 describes the throughput of the side channel with one subcarrier being erased in each OFDM symbol. The side channel could achieve a throughput higher than 1 Mbps with BPSK when the SNR is higher than 8 dB. The maximum data rate of 1.25 Mbps can be approached when the SNR is higher than 16 dB. Furthermore, according to Table 2, our side channel can achieve a minimal data throughput at 350 Kbps, which is more than four times higher than the maximal VoIP data rate from ITU-T standard [1].

Furthermore, when two subcarriers are erased in each OFDM symbol, the minimum SNR required to achieve 95 percent of the maximum throughput of 2.5 Mbps is shown in Table 3. Compared to Table 2, at least another 3 dB is required in the channel SNR to maximize the data throughput.

TABLE 1
Side Channel Detection Rate with a 9 Mbps Data Rate

SNR (dB)	4	6	8	10	12	14	16
Basic approach (1)	0.22	0.45	0.72	0.90	0.98	0.99	1.00
Prob. approach (1)	0.34	0.61	0.84	0.93	0.98	0.99	1.00
Basic approach (2)	0.07	0.24	0.56	0.86	0.96	0.98	1.00
Prob. approach (2)	0.18	0.42	0.74	0.90	0.97	0.98	1.00

TABLE 2
Side Channel Throughput (Mbps) with One Subcarrier Being Erased in Each OFDM Symbol

SNR (dB)	4	8	12	16	24	30
BPSK	0.781	1.170	1.213	1.233	1.235	1.235
QPSK	0.784	1.176	1.237	1.226	1.235	1.225
16-QAM	0.397	0.807	1.116	1.186	1.188	1.210
64-QAM	0.350	0.620	0.888	1.101	1.157	1.200

6.5 Impacts on the Main Channel

The encoded information conveyed by the subcarriers being erased is entirely discarded, which will inevitably have impacts on the capability of noise resistance of the main channel. To evaluate the impact of our side channel design on the main channel, we enforce the side channel to the main channel when the main channel has a BER of 1 percent, and then evaluate the increase of the main channel BER due to the existence of the side channel. The results are shown in Fig. 10. Since our proposed design is able to appropriately control the amount of patterned interference being applied to the main channel, we are able to limit the increase of the main channel BER within 0.6 percent, and hence retain the performance of the main channel in various practical scenarios.

The BER increase under different SNR conditions in the main channel is shown in Fig. 10b. Such increase could be efficiently controlled between 2 to 4 percent for all the eight possible data rates being used in WiFi networks. By comparing Fig. 10b with Fig. 1, we notice that the BER increase only exceeds 1 percent when the channel SNR is lower than the required SNR to support the corresponding data rate. For example, the BER increase for 64-QAM (54 Mbps) is only noticeable when the channel SNR is lower than 17.5 dB, which is much lower than the required 26.7 dB to support 64-QAM [49]. Therefore, in most of practical scenarios, the existence of the side channel produces only negligible impacts on the main channel. Such small BER increase, on the other hand, retains the packet delivery rate at the same communication distance. The communication range of wireless networks, hence, will not be affected by the operation of the side channel.

6.6 Accuracy of Preamble Detection

In this section, we evaluate our proposed design of connection establishment and transmission control in Section 5. In our experiment, we adjust the parameter D from 10 samples ($0.5\,\mu s$) to 30 samples ($1.5\,\mu s$). The misdetection ratio, as shown in Fig. 11a, can be efficiently controlled below

TABLE 3
SNR Requirement with Two Subcarriers Being Erased in Each OFDM Symbol

Modulation type	BPSK	QPSK	16-QAM	64-QAM
Minimum SNR (dB)	13	15	20	27

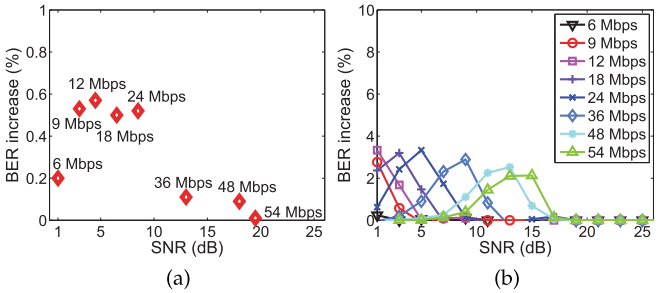

Fig. 10. Impact on the main channel: (a) BER increase under 1 percent main channel BER; (b) BER increase under different SNR conditions.

1 percent when SNR is higher than 10 dB, and only increases to more than 20 percent when SNR is lower than 5 dB.

On the other hand, we also evaluate the false addressing ratio, which is defined as the percentage of incorrect interpretation of the address information being encoded in the preamble. The evaluation results are shown in Fig. 11b. The addressing error is mainly resulted from the timing inaccuracy of the internal clock at the WiFi receiver, and hence can be eliminated by increasing D. When the value of D increases, the system is more tolerant to channel noise and reduces the false addressing ratio, at a cost of a smaller addressing space being supported. Also, the false addressing ratio can be efficiently suppressed below 1 percent when SNR exceeds 10 dB. Given that 10 dB is the minimum SNR required to maintain a WiFi connection in practice [49], we prefer to use $D = 10$ in our real application and hence allow 6-bit addresses being encoded into the preamble.

6.7 Power Consumption of the Side Channel

Theoretically, subcarrier erasure reduces the RF power consumed by the WiFi frontend, and the side channel, hence, incurs limited additional overhead to wireless network operations. In practice, since it is difficult to directly measure the power consumed by the RF frontend on USRP daughterboard, we instead measure the total power consumed by a USRP board that also includes the power consumed by power ICs, FPGA cores and so on. We use a DC power supplier HY3005F-3 to power up the USRP with 6 V fixed voltage supply, and evaluate the power consumption by measuring the current. Our experimental results show that, when a USRP board is in idle status, it draws 2.29A from the power supply. A running 802.11a system between two USRP boards, then, increases such energy consumption to 2.62A. However, when we further apply the side channel onto the WiFi transceiver and increase the number of erased OFDM subcarriers in each symbol from 0 to 3, there is not any noticeable change on the power consumption. Since the resolution of power measurement of the power supply we use is 10 mA, we conclude that the power consumption if the side channel is negligible compared to the main channel (2.62A-2.29A = 330 mA). In the future, we will adopt a testing device with a higher measurement resolution to investigate the exact power consumption of the side channel.

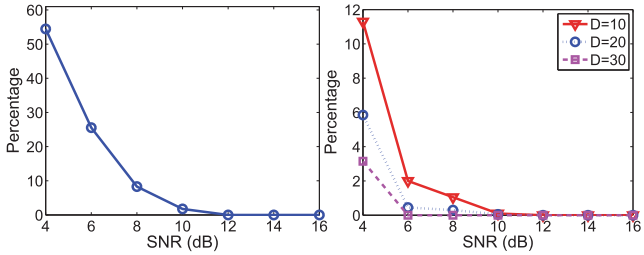

Fig. 11. Accuracy of preamble detection with additional preamble.

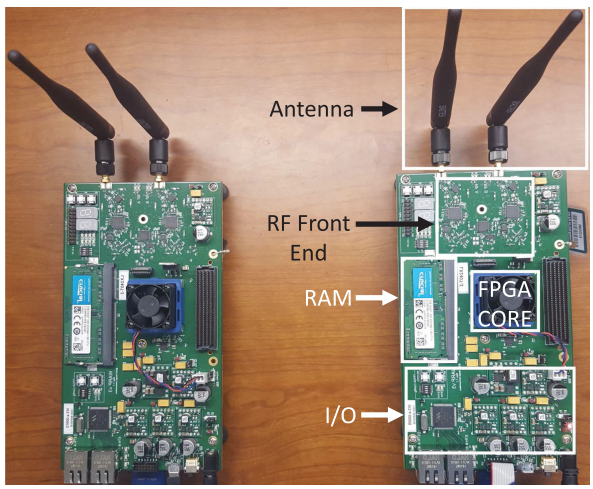

Fig. 12. Warp3 platform.

7 Hardware Implementation

In order to evaluate our proposed side channel design over more realistic wireless scenarios, we also implemented our side channel design over WARP v3 board, which is a FPGA-based wireless hardware platform. It allows hardware-based implementation of a fully functional wireless transceiver over its FPGA core [15] as show in Fig. 12. It hence allows real-time wireless networking and full compatibility with commodity wireless devices: since all the Tx and Rx operations are being conducted over the FPGA hardware instead of via GNU software emulation, it incurs near-zero computation delay to our proposed side channel operation for simulating the performance in commodity wireless devices.

On the other hand, our implementation only requires the minimum modification to the existing wireless system hardware. More specifically, our design only adds one extra subsystem to the commodity WiFi PHY with the minimum complexity, by applying only few multiplexers and multipliers to the WiFi hardware chip. In our implementation over the WARP boards, this extra subsystem only introduces 0.001 percent more usage of the WARP board's FPGA logic resources and 50 ns additional computational delay, as discussed and evaluated in Sections 7.2 and 8.3.

7.1 Implementation Overview

The architecture of our hardware implementation of the side channel design is shown in Fig. 13. Based on the

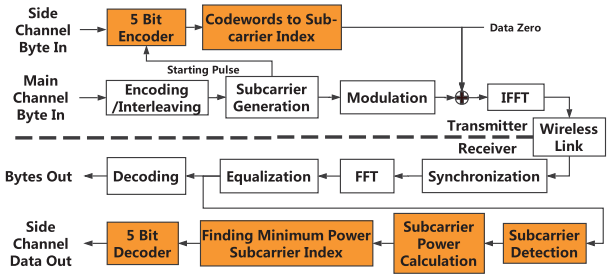

Fig. 13. Side channel implementation over WARP.

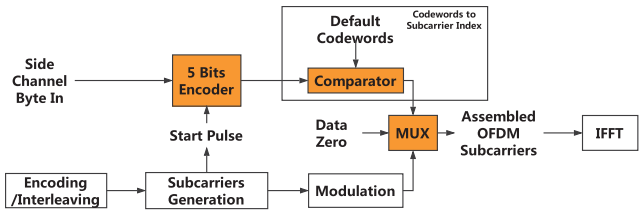

Fig. 14. Details of Tx design over WARP.

original 802.11 PHY structure, the added side channel subsystem is highlighted in color. It does not affect any existing modules in the existing 802.11 PHY, but instead adds new sub-blocks after channel modulation in the Tx side and channel equalization in the Rx side.

At the Tx side, the side channel block is added when the main channel's modulation starts after its OFDM subcarriers are generated. The side channel block is operating in parallel with the modulation block in the main channel. In the side channel, the input data stream will build a data codeword with every 5 data bits, and this side channel codeword represents the location of subcarrier to be erased in the main channel. Afterwards, the I/Q data for this subcarrier in the main channel will be changed to zero, indicating erasure of subcarrier energy. Details will be described in Section 7.2.

At the Rx side, after the received RF signal passes through channel equalization, a subsystem for detecting the index of subcarrier with the minimum power in the received OFDM symbols is added to the original 802.11 receiver, and the side channel codeword is then represented by the subcarrier index with the lowest power. In our implementation, the main channel subcarrier with the minimum power is decided by comparing the I/Q signal of the OFDM symbol in different the main channel subcarriers. Finally, a 5-bit hardware decoder is used to convert the side channel codeword to side channel data.

7.2 Delay Reduction

Adding the side channel operation to erase the subcarrier energy in the existing 802.11 system may incur additional computational delay on the Tx side. Such delay in FPGA design is represented by clock cycles, i.e., the amount of main clock cycles that are needed to process each side channel codeword.

To minimize such delay, as shown in Fig. 14, we strive to implement the side channel Tx by solely using comparators and multiplexers that introduces no extra delay in hardware, and avoid using blocks of multipliers or adders, each of which adds three extra clock cycles of delay into the design over the Virtex-6 FPGA core on WARP v3. More specifically, as shown in Fig. 14, we pre-load the entire set of 32 possible 5-bit codewords (i.e., 00000 to 11111) in the on-board RAM of WARP. A comparator that compares the side channel codeword with the pre-load codewords is then used to find out which codeword is actually being transmitted in the side channel. Afterwards, instead of using a multiplier, we use a multiplexer (MUX) to apply signal '0' to the corresponding main channel subcarrier by replacing the original signal in that subcarrier. In this way, we can effectively reduce the delay caused by the side channel computation to zero in theory on Tx.

However, multipliers will be required at the Rx side to calculate the power in each main channel subcarrier from its I/Q signal. Therefore, the additional computation delay at the Rx side is inevitable, and we will experimentally evaluate such delay in Section 8.3.

7.3 Channel Symbol Synchronization

Another crucial issue in our implementation is how to precisely synchronize between the side channel and the main channel. If they are not synchronized, the side channel codeword will be mapped to wrong subcarriers in the main channel and result in serious bit errors. However, the accuracy of such synchronization is generally difficult to be ensured at FPGA, because the generation of the main channel subcarriers and PHY-layer mapping of the side channel codewords could take different amounts of computational time at the FPGA core of WARP.

To solve this problem, as shown in Fig. 14, our system asserts a starting pulse after the first symbol is generated in the main channel. This starting pulse is sent to the side channel block for synchronization, and the generation of the side channel codewords will then be triggered by this pulse. Since the main channel modulation takes negligible computational delay after the rising edge of the starting pulse, and generation of the side channel codewords also produces zero computation delay according to Section 7.2, they can be precisely synchronized with each other.

8 Performance Evaluation over Wireless Hardware

Built on our hardware implementation in Section 7, we further evaluate the performance of our side channel design over the 2.4 GHz frequency band in practical wireless scenarios, in which the wireless network may be unexpectedly interfered by concurrent wireless transceivers or disrupted due to various environmental uncertainty.

8.1 Experiment Setup

Our experiments are solely operated by the WARP v3 boards without the help of host PC. In our experiments, packets with random payload of 1,400 bytes are constantly transmitted in the main channel, and one subcarrier among the 52 OFDM data subcarriers in each symbol of the main channel is exploited as the side channel. To test the performance of our design under different channel conditions, we tune the Tx gain on WARP transceivers from −9 to 11 dB, to achieve a maximum main channel SNR at 23 dB. To evaluate the communication and computation overhead of the side channel operations, each WARP board is connected to a laptop PC with Intel 4720HQ 2.6 Ghz and 16 Gb of memory through an ethernet cable at 1 Gbps. All the experiment results are averaged over multiple experiment runs under different indoor setup for statistical convergence.

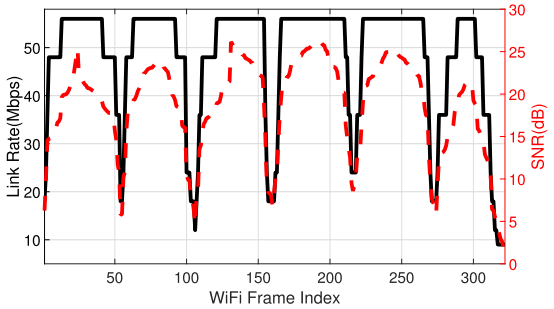

(a) Main channel Link Rate

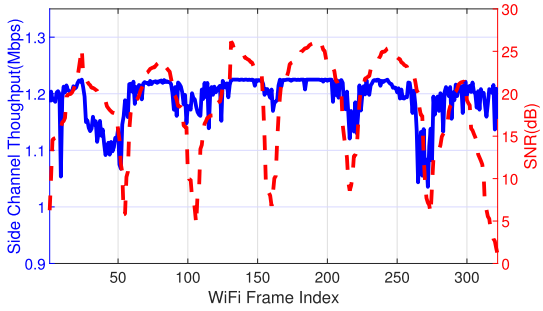

(b) Side Channel Throughput

Fig. 15. Side channel and main channel performance with fluctuating main channel data rate.

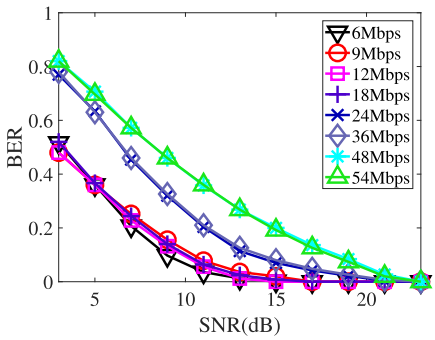

Fig. 16. Side channel BER in the 2.4 GHz channel.

8.2 Side Channel Performance

In this section, we evaluate the performance of our side channel design in the more commonly used 2.4 GHz frequency band. Our experiment is conducted between two WARP boards, one of which serves as the wireless access point (AP) and provides wireless access in the 2,414 MHz channel with different modulation schemes.

We first evaluate the side channel performance with rate adaption. Fig. 15a shows how the main channel's link rate fluctuates when the main channel SNR varies. Correspondingly, Fig. 15b shows the side channel performance under such fluctuation. When the main channel's data rate drops to 9 and 12 Mbps under poor channel SNR conditions, the side channel throughput is still as high as 1.07 Mpbs. Fig. 15b also shows that the side channel has at least 89 percent of its maximum throughput under all SNR conditions, and demonstrates that our design can maintain the side channel throughput even with highly dynamic main channel conditions.

As shown in Fig. 16, the side channel BER steadily drops when the main channel SNR improves. When the main channel SNR is greater than 12 dB, the side channel BER is lower than 5 percent with BPSK and QPSK modulation. When the main channel SNR is higher than 19 dB, the side channel BER is lower than 5 percent for all modulation schemes. Furthermore, Fig. 17 shows that the main channel throughput suffers little performance loss from the existence of the side channel, and retains more than 98.5 percent of its original throughput. In particular, when different modulation schemes apply in the main channel, the loss in the throughput is negligible.

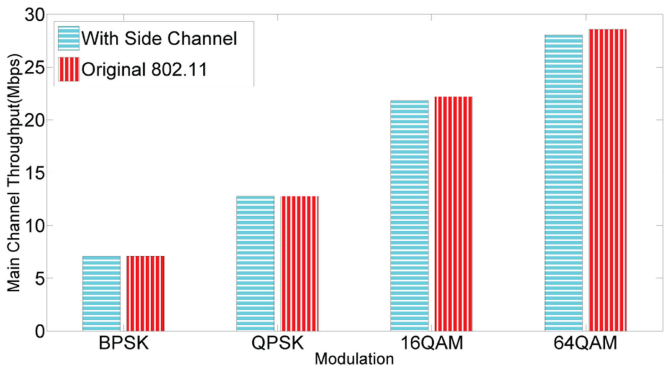

Fig. 17. Main channel throughput with different modulation scheme.

In our experiments, we observed a 5 percent difference in the side channel BER, when comparing our results with the results under the same main channel SNR obtained in Section 6.3 over the 5 GHz band. The primary reason for such difference is that the 2.4 GHz band is more commonly used and hence has more interference from surrounding wireless devices. Such difference may also be caused by the RF heterogeneity of different wireless transceivers being used in experiments. Generally speaking, we conclude that our side channel design has a consistent performance over both 2.4 and 5 Ghz wireless channels.

8.3 Computation Delay and Overhead

In this section, we evaluate extra computation delay caused by the side channel operation at the wireless PHY. As we stated in Section 7.2, the side channel Rx will introduce 8 additional clock cycles to finish due to the involvement of multipliers. With a 160 Mhz main clock on the WARP v3 board, such delay brought by the side channel operation is 50 ns at the receiver.

Based on such result, we can further evaluate the extra processing power required by the side channel operations. Since we implemented the side channel over WARP's FPGA core as slices with basic digital logic blocks such as LUTs, flip-flops and carry logic elements, we can measure such computation overhead as the amount of slice registers being used in the FPGA implementation. More specifically, the Virtex-6 FPGA on the WARP v3 board has 37,680 slices of configurable logic blocks, and our side channel implementation only introduces only 0.001 percent more usage of these computational resources.

8.4 Impact of Channel Interference

To further investigate the performance of our side channel design in practical wireless scenarios with strong interference, we introduce a third WARP node running as an original WiFi AP into experiments, and place it between the two other wireless transceivers that operate the side channel. This node is configured to keep broadcasting dumb data over the same frequency band where the main channel is operated. As

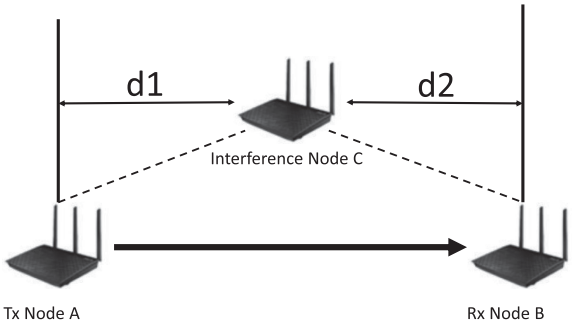

Fig. 18. Nodes placement.

TABLE 4
Channel Throughput (Mbps)

Modulation	BPSK	QPSK	16-QAM	64-QAM
Main channel	5.4 (6.85)	8.19 (12.54)	11.68 (17.97)	13.99 (25.46)
Side channel	1.22 (1.22)	1.22 (1.22)	1.21 (1.21)	1.20 (1.19)

Numbers in brackets are the throughput without interference.

shown in Fig. 18, the amount of channel interference could be then controlled by varying the distances $d1$ and $d2$ between the three wireless nodes.

In the first experiment, we set $d1 = 3\,\mathrm{m}$ and $d2 = 0.15\,\mathrm{m}$, and the Tx power for node C is set to 15 dBm. We then evaluate the main channel and the side channel throughputs at the same time. Table 4 lists the maximal throughputs in the side channel and the main channel, respectively, and shows that the main channel throughput can suffer up to 55 percent degradation with 64-QAM modulation, compared to that without interference. On the contrary, the side channel throughput remains at the same level, and we only witness a maximum of 1 percent performance loss with 64-QAM. This result shows that when the main channel throughput is greatly impacted by the interference, the impact of throughput on the side channel is negligible.

Furthermore, we increase $d1$ to 7 m, so that the wireless interference from C is relatively even stronger at the side channel receiver B. We fixed the A's transmission power and B's receiver gain at the same level of -5 dB, which gives the channel SNR around 9 dB at B. According to the results shown in Fig. 19, when 64-QAM modulation is used in the main channel, the side channel BER could increase by 7 percent. For all other modulation schemes used in the main channel, our design could effectively restrain the BER increase within 5 percent. Considering the low levels of the side channel BER, the impact of channel interference on the side channel operation is nearly negligible. These experiment results show that, in most of the practical environments, the extra wireless transciever will have negligible impact on our side channel operation, even when the main channel performance is heavily impacted by the interference.

9 Discussions

9.1 Reducing the Main Channel BER

In our current design of the wireless side channel, erasing OFDM subcarriers will inevitably result in data loss and BER increase in the main channel. Our experiment results in Section 6.5 have shown that the existence of the side channel

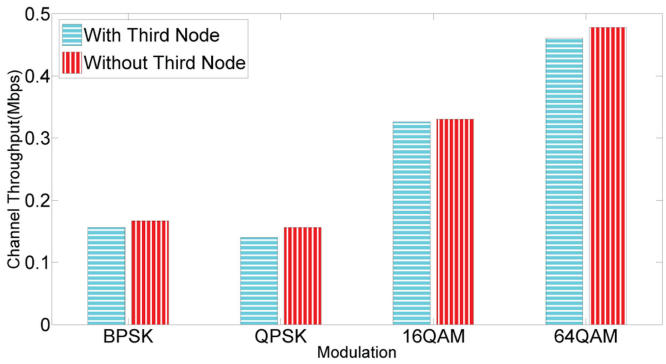

Fig. 19. Side channel BER with wireless interference. Tx power is set as -5 dB.

could potentially increase the BER of the main channel by up to 1 percent in practical scenarios. To better understand such increase of the main channel BER, we categorize the patterned interference being applied on the main channel into two groups, i.e., the destructive interference and non-destructive interference. In destructive interference design such as Flashback [8] and our current design, the entire OFDM subcarrier is interfered, and we are unable to estimate the original waveform in the interfered subcarrier from the interfered signal. Although this design reduces the complexity of interference detection and the operations of the side channel, it raises more challenge to reduce the main channel BER.

On the other hand, a design based on non-destructive interference allows estimation of the original signal waveform in the interfered subcarrier from the received signal. A viable solution to such estimation is to interpolate weak interference to an OFDM subcarrier. Such interpolation, however, requires the design of a highly robust signal and a channel detector, especially in low SNR scenarios. Such robustness could be possibly achieved by exploiting the interference cancellation techniques which cancel the intended interference and recover the information being interfered [53].

9.2 Further Improvement of Side Channel Throughput

Another limitation of our current design is that, the designated throughput of the side channel remains constant in different SNR scenarios. In other words, the increase of channel SNR does not benefit the side channel, whose data rate is limited by the elapsed time of an OFDM symbol. However when the channel SNR is sufficiently high, interference that is weaker than energy erasure could also be possibly detected. The throughput of the side channel, may increased by appending more interference. To further increase such throughput, a modulation approach in the side channel based on non-destructive interference is desired, and a new data rate adaptation mechanism should be introduced in the side channel to take the channel SNR condition and the modulation scheme in the main channel into account. Under good SNR conditions, a viable solution is to utilize minimum but detectable non-destructive interference to intentionally interfere each subcarrier in an OFDM symbol, which yields a big increase in the side channel throughput.

9.3 Multiple-Access Side Channels

Our side channel design being proposed in this paper requires that the side channel and the main channel are

operated by the same wireless device. In many practical application scenarios such as large-scale IoTs, however, multiple wireless devices may transmit delay-sensitive data traffic simultaneously. Hence, these devices will require multiple access to the side channel. Designing such multiple-access side channels is challenging due to the following reasons. First, when the side channel and the main channel are operated by different wireless devices, the RF signal of the side channel will be appended to the main channel signal as extra interference, and it is hence difficult to demodulate the side channel data being transmitted from the mixed signal. Second, the side channel signal has to be transmitted with much weaker power to minimize its impact on the main channel. This reduction in Tx power lowers the side channels effective SNR and increases the error rate of data demodulation. These challenges need further modifications to the side channel design, and such modifications will be our future work.

9.4 Correlation with Wireless Packet Scheduling

Wireless parket scheduling algorithms, such as Improved Channel State Dependent Packet Scheduling (I-CSDPS) [13] and Channel-condition Independent packet Fair Queueing (CIF-Q) [39], aim to maximize the wireless system capacity by allocating transmission opportunities among different wireless users in the network. However, such scheduling can only be done after CSMA resolved the packet collision and link congestion in the wireless channel, and hence has limited capability of addressing the link delay due to users' contention for channel access. Furthermore, as more users competing for the limited channel resource, the delay from packet scheduling will increase significantly due to the increasing CSMA back-off time, and the efficiency of such packet scheduling will surely drop. On the contrary, data traffic being transmitted in the side channel will not be impacted by such link congestion in anyway, and instead only experiences the link propagation delay.

Furthermore, the major focus of our side channel design is orthogonal to wireless link scheduling algorithms, such as Maximum Weight Scheduling (MWS) [48] and distributed greedy (DistGreedy) [20] algorithm. These algorithms focus on reducing the total queuing delay in a multi-hop wireless network, and hence require global information about the conditions of multiple wireless links. In contrast, our side channel design aims to reduce the transmission delay in a single wireless link.

10 Conclusion

In this paper, we present a novel design of high-throughput wireless side channel, which efficiently supports real-time wireless traffic without consuming any additional wireless spectrum resource. The basic idea of our side channel design is to exploit the SNR margin in the main channel to encode data as patterned interference, and realize such patterned interference as energy erasure over OFDM subcarriers. We have implemented and evaluated the side channel design over practical SDR platforms and FPGA based hardware platform. The experiment results verify the effectiveness of the side channel in reducing the data transmission latency and providing a data throughput higher than 1 Mbps, with minimum impact on the performance of the main wireless channel. Our future work will incorporate the proposed side channel design into latest wireless network standards, such as 802.11n and 802.11ac.

Acknowledgments

This work was supported in part by the US National Science Foundation (NSF) under grants CNS-1826884, CNS-1812399 and CNS-1812407. The first two co-authors made equal contributions to this paper.

References

[1] Pulse code modulation (PCM) of voice frequencies. [Online]. Available: https://www.itu.int/rec/T-REC-G.711/en
[2] *Part 11: Wireless LAN Medium Access Control (MAC) and Physical Layer (PHY) Specifications*, IEEE Standard 802.11–2012, Mar. 2012.
[3] A. Amiri Sani, K. Boos, M. H. Yun, and L. Zhong, "Rio: A system solution for sharing I/O between mobile systems," in *Proc. ACM Annu. Int. Conf. Mobile Syst. Appl. Services*, 2014, pp. 386–386.
[4] G. Bianchi, L. Fratta, and M. Oliveri, "Performance evaluation and enhancement of the CSMA/CA MAC protocol for 802.11 wireless LANs," in *Proc. 7th IEEE Int. Symp. Pers. Indoor Mobile Radio Commun.*, 1996, pp. 392–396.
[5] L. Chen and W. B. Heinzelman, "QoS-aware routing based on bandwidth estimation for mobile ad hoc networks," *IEEE J. Sel. Areas Commun.*, vol. 23, no. 3, pp. 561–572, Mar. 2005.
[6] Z. Chi, Y. Li, H. Sun, Y. Yao, Z. Lu, and T. Zhu, "B2W2: N-way concurrent communication for IoT devices," in *Proc. ACM Conf. Embedded Netw. Sensor Syst. CD-ROM*, 2016, pp. 245–258.
[7] D.-M. Chiu and R. Jain, "Analysis of the increase and decrease algorithms for congestion avoidance in computer networks," *Comput. Netw. ISDN Syst.*, vol. 17, pp. 1–14, 1989.
[8] A. Cidon, K. Nagaraj, S. Katti, and P. Viswanath, "Flashback: Decoupled lightweight wireless control," in *Proc. ACM SIGCOMM Conf. Appl. Technol. Archit. Protocols Comput. Commun.*, 2012, pp. 223–234.
[9] I. Demirkol, C. Ersoy, F. Alagoz, et al., "MAC protocols for wireless sensor networks: A survey," *IEEE Commun. Mag.*, vol. 44, no. 4, pp. 115–121, Apr. 2006.
[10] M. Ergen, S. Coleri, and P. Varaiya, "QoS aware adaptive resource allocation techniques for fair scheduling in OFDMA based broadband wireless access systems," *IEEE Trans. Broadcast.*, vol. 49, no. 4, pp. 362–370, Dec. 2003.
[11] W. Gao, Y. Li, H. Lu, T. Wang, and C. Liu, "On exploiting dynamic execution patterns for workload offloading in mobile cloud applications," in *Proc. IEEE Int. Conf. Netw. Protocols*, 2014, pp. 1–12.
[12] Y. Geng, W. Hu, Y. Yang, W. Gao, and G. Cao, "Energy-efficient computation offloading in cellular networks," in *Proc. IEEE Int. Conf. Netw. Protocols*, 2015, pp. 145–155.
[13] J. Gomez, A. T. Campbell, and H. Morikawa, "The Havana framework for supporting application and channel dependent QoS in wireless networks," in *Proc. 7th Int. Conf. Netw. Protocols*, 1999, pp. 235–244.
[14] A. Gudipati and S. Katti, "Strider: Automatic rate adaptation and collision handling," in *Proc. ACM SIGCOMM Conf.*, 2011, pp. 158–169.
[15] S. Gupta, C. Hunter, P. Murphy, and A. Sabharwal, "WARPNet: Clean slate research on deployed wireless networks," in *Proc. 10th ACM Int. Symp. Mobile Ad Hoc Netw. Comput.*, 2009, pp. 331–332.
[16] K. Ha, Z. Chen, W. Hu, W. Richter, P. Pillai, and M. Satyanarayanan, "Towards wearable cognitive assistance," in *Proc. ACM Annu. Int. Conf. Mobile Syst. Appl. Services*, 2014, pp. 68–81.
[17] G. Holland, N. Vaidya, and P. Bahl, "A rate-adaptive MAC protocol for multi-hop wireless networks," in *Proc. 7th Annu. Int. Conf. Mobile Comput. Netw.*, 2001, pp. 236–251.
[18] B. Hull, K. Jamieson, and H. Balakrishnan, "Mitigating congestion in wireless sensor networks," in *Proc. 2nd Int. Conf. Embedded Netw. Sensor Syst.*, 2004, pp. 134–147.
[19] A. P. Jardosh, K. N. Ramachandran, K. C. Almeroth, and E. M. Belding-Royer, "Understanding congestion in IEEE 802.11 B wireless networks," in *Proc. 5th ACM SIGCOMM Conf. Internet Meas.*, 2005, pp. 25–25.
[20] C. Joo, X. Lin, J. Ryu, and N. B. Shroff, "Distributed greedy approximation to maximum weighted independent set for scheduling with fading channels," in *Proc. 14th ACM Int. Symp. Mobile Ad Hoc Netw. Comput.*, 2013, pp. 89–98.
[21] J. Zhang, X. Zhang, P. Kulkarni, and P. Ramanathan, "OpenMili: A 60 GHz software radio platform with a reconfigurable phased-array antenna," in *Proc. 22nd Annu. Int. Conf. Mobile Comput. Netw.*, 2017.

[22] S. M. Kim and T. He, "FreeBee: Cross-technology communication via free side-channel," in *Proc. 21st Annu. Int. Conf. Mobile Comput. Netw.*, 2015, pp. 317–330.
[23] Z.-N. Kong, D. H. Tsang, B. Bensaou, and D. Gao, "Performance analysis of IEEE 802.11e contention-based channel access," *IEEE J. Sel. Areas Commun.*, vol. 22, no. 10, pp. 2095–2106, Dec. 2004.
[24] J. F. Kurose and K. W. Ross, *Computer Networking: A Top-Down Approach*, 6th ed. London, U.K.: Pearson, 2012.
[25] L. Deek, E. Garcia-Villegas, E. Belding, S.-J. Lee, and K. Almeroth, "Intelligent channel bonding in 802.11n WLANs," *IEEE Trans. Mobile Comput.*, vol. 13, no. 6, pp. 1242–1255, Jun. 2014.
[26] L. B. Le, E. Modiano, and N. B. Shroff, "Optimal control of wireless networks with finite buffers," *IEEE/ACM Trans. Netw.*, vol. 20, no. 4, pp. 1316–1329, Aug. 2012.
[27] K. Lee, D. Chu, E. Cuervo, A. Wolman, and J. Flinn, "Demo: DeLorean: Using speculation to enable low-latency continuous interaction for mobile cloud gaming," in *Proc. ACM Annu. Int. Conf. Mobile Syst. Appl. Services*, 2014, pp. 347–347.
[28] Y. Li and W. Gao, "Code offload with least context migration in the mobile cloud," in *Proc. IEEE INFOCOM*, 2015, pp. 1876–1884.
[29] Y. Li and W. Gao, "MUVR: Supporting multi-user mobile virtual reality with resource constrained edge cloud," in *Proc. IEEE/ACM Symp. Edge Comput.*, 2018, pp. 1–16.
[30] Y. Li and W. Gao, "DeltaVR: Achieving high-performance mobile VR dynamics through pixel reuse," in *Proc. 18th Int. Conf. Inf. Process. Sensor Netw.*, 2019, pp. 13–24.
[31] Z. Li and T. He, "WEBee: Physical-layer cross-technology communication via emulation," in *Proc. ACM Annu. Int. Conf. Mobile Comput. Netw.*, 2017, pp. 2–14.
[32] Z. Liu, Y. Xin, and G. B. Giannakis, "Linear constellation precoding for OFDM with maximum multipath diversity and coding gains," *IEEE Trans. Commun.*, vol. 51, no. 3, pp. 416–427, Mar. 2003.
[33] R. Love, R. Kuchibhotla, A. Ghosh, R. Ratasuk, B. Classon, and Y. Blankenship, "Downlink control channel design for 3GPP LTE," in *Proc. IEEE Wireless Commun. Netw. Conf.*, 2008, pp. 813–818.
[34] H. Lu and W. Gao, "Scheduling dynamic wireless networks with limited operations," in *Proc. IEEE 24th Int. Conf. Netw. Protocols*, 2016, pp. 1–10.
[35] H. Lu and W. Gao, "Continuous wireless link rates for internet of things," in *Proc. 17th ACM/IEEE Int. Conf. Inf. Process. Sensor Netw.*, 2018, pp. 48–59.
[36] E. Magistretti, K. K. Chintalapudi, B. Radunovic, and R. Ramjee, "WiFi-Nano: Reclaiming WiFi efficiency through 800 ns slots," in *Proc. ACM Annu. Int. Conf. Mobile Comput. Netw.*, 2011, pp. 37–48.
[37] P. Mohapatra and S. Krishnamurthy, *AD HOC NETWORKS: Technologies and Protocols*. Berlin, Germany: Springer, 2004.
[38] R. Nee, "Breaking the Gigabit-per-second barrier with 802.11AC," *IEEE Wireless Commun.*, vol. 18, no. 2, pp. 4–4, Apr. 2011.
[39] T. E. Ng, I. Stoica, and H. Zhang, "Packet fair queueing algorithms for wireless networks with location-dependent errors," in *Proc. 7th Annu. Joint Conf. IEEE Comput. Commun. Societies*, 1998, pp. 1103–1111.
[40] D. R. Pauluzzi and N. C. Beaulieu, "A comparison of SNR estimation techniques for the AWGN channel," *IEEE Trans. Commun.*, vol. 48, no. 10, pp. 1681–1691, Oct. 2000.
[41] T. M. Schmidl and D. C. Cox, "Robust frequency and timing synchronization for OFDM," *IEEE Trans. Commun.*, vol. 45, no. 12, pp. 1613–1621, Dec. 1997.
[42] W.-L. Shen, K. C.-J. Lin, S. Gollakota, and M.-S. Chen, "Rate adaptation for 802.11 multiuser MIMO networks," *IEEE Trans. Mobile Comput.*, vol. 13, no. 1, pp. 35–47, Jan. 2014.
[43] O. Simeone, Y. Bar-Ness, and U. Spagnolini, "Pilot-based channel estimation for OFDM systems by tracking the delay-subspace," *IEEE Trans. Wireless Commun.*, vol. 3, no. 1, pp. 315–325, Jan. 2004.
[44] S. Kumar, D. Cifuentes, S. Gollakota, and D. Katabi, "Bringing cross-layer MIMO to today's wireless LANs," *ACM SIGCOMM Comput. Commun. Rev.*, vol. 43, pp. 387–398, 2013.
[45] S. Sur, I. Pefkianakis, X. Zhang, and K.-H. Kim, "WiFi-assisted 60 GHz wireless networks," in *Proc. 23rd Annu. Int. Conf. Mobile Comput. Netw.*, 2017, pp. 28–41.
[46] H. Sugiyama and K. Nosu, "MPPM: A method for improving the band-utilization efficiency in optical PPM," *J. Lightw. Technol.*, vol. 7, no. 3, pp. 465–472, Mar. 1989.
[47] K. Sui, M. Zhou, D. Liu, M. Ma, D. Pei, Y. Zhao, Z. Li, and T. Moscibroda, "Characterizing and improving WiFi latency in large-scale operational networks," in *Proc. 14th Annu. Int. Conf. Mobile Syst. Appl. Services*, 2016, pp. 347–360.
[48] L. Tassiulas and A. Ephremides, "Stability properties of constrained queueing systems and scheduling policies for maximum throughput in multihop radio networks," *IEEE Trans. Autom. Control*, vol. 37, no. 12, pp. 1936–1948, Dec. 1992.
[49] J. Thomson, B. Baas, E. M. Cooper, J. M. Gilbert, G. Hsieh, P. Husted, A. Lokanathan, J. S. Kuskin, D. McCracken, B. McFarland, et al., "An integrated 802.11a baseband and MAC processor," in *Proc. IEEE Int. Solid-State Circuits Conf.*, 2002, pp. 126–451.
[50] L. Tong and W. Gao, "Application-aware traffic scheduling for workload offloading in mobile clouds," in *Proc. IEEE INFOCOM*, 2016, pp. 1–9.
[51] L. Tong, Y. Li, and W. Gao, "A hierarchical edge cloud architecture for mobile computing," in *Proc. IEEE INFOCOM*, 2016, pp. 1–9.
[52] T. Wild, F. Schaich, and Y. Chen, "5G air interface design based on universal filtered (UF-)OFDM," in *Proc. IEEE 19th Int. Conf. Digit. Signal Process.*, 2014, pp. 699–704.
[53] K. Wu, H. Li, L. Wang, Y. Yi, Y. Liu, Q. Zhang, and L. Ni, "HJam: Attachment transmission in WLANs," in *Proc. IEEE INFOCOM*, 2012, pp. 1449–1457.
[54] K. Wu, H. Tan, Y. Liu, J. Zhang, Q. Zhang, and L. Ni, "Side channel: Bits over interference," in *Proc. ACM Annu. Int. Conf. Mobile Comput. Netw.*, 2010, pp. 13–24.
[55] B. Yang, K. Letaief, R. S. Cheng, and Z. Cao, "Channel estimation for OFDM transmission in multipath fading channels based on parametric channel modeling," *IEEE Trans. Commun.*, vol. 49, no. 3, pp. 467–479, Mar. 2001.
[56] X. Zhang and K. G. Shin, "E-MiLi: Energy-minimizing idle listening in wireless networks," in *Proc. ACM Annu. Int. Conf. Mobile Comput. Netw.*, 2011, pp. 205–216.
[57] X. Zhang and K. G. Shin, "Gap sense: Lightweight coordination of heterogeneous wireless devices," in *Proc. IEEE INFOCOM*, 2013, pp. 3094–3101.

Ruirong Chen (S'17) received the BE degree majoring in electrical and computer engineering from the Harbin Institute of Technology, in 2015. Currently, he is working toward the PhD degree in the Department of Electrical and Computer Engineering, University of Pittsburgh, Pittsburgh. His research interests include wireless network systems and wireless sensing. He is a student member of the IEEE.

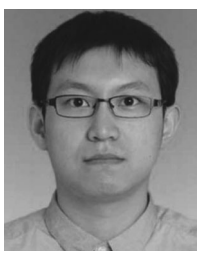

Haoyang Lu (S'15) received the BE degree in electrical engineering from Hangzhou Dianzi University, in 2010, and the ME degree in electrical engineering from the University of Chinese Academy of Sciences, in 2013. He is currently working toward the PhD degree in the Department of Electrical Engineering and Computer Science, University of Tennessee, Knoxville. His research interests include smart grid and communication system. He is a student member of the IEEE.

Wei Gao (M'05) received the BE degree in electrical engineering from the University of Science and Technology of China, in 2005, and the PhD degree in computer science from Pennsylvania State University, in 2012. He is currently an associate professor with the Department of Electrical and Computer Engineering, University of Pittsburgh. His research interests include wireless networking, mobile and embedded computing systems, Internet of Things, and cyber-physical systems. He received the U.S. National Science Foundation (NSF) CAREER award in 2016. He is a member of the IEEE.